Original Research Paper

# Linear-like polypeptide-based micelle with pH-sensitive detachable PEG to deliver dimeric camptothecin for cancer therapy

*Ka Hong Wong [a,1], Zhaopei Guo [a,1], Di Jiang [a], Xingzhi Zhou [a], Lizhu Lin [b], Denggao Zhao [c], Meiwan Chen [a,*]*

[a] *State Key Laboratory of Quality Research in Chinese Medicine, Institute of Chinese Medical Sciences, University of Macau, Macau 999078, China*
[b] *The First Affiliated Hospital of Guangzhou University of Chinese Medicine, Guangzhou 510407, China*
[c] *School of Biotechnology and Health Sciences, Wuyi University, Jiangmen 529020, China*

ARTICLE INFO

ABSTRACT

Nano drug delivery systems have made significant progress in delivering anticancer drugs camptothecin (CPT). However, many challenges for CPT delivery remain, including low drug loading efficiency, premature drug leakage, and poor cellular internalization. Herein, we report a novel dual-sensitive polypeptide-based micelle with remarkably high drug loading of CPT for cancer therapy. This self-assembled micelle possesses the following essential components for CPT: (1) pH-sensitive PEG (OHC-PEG-CHO) for prolonging blood circulation and allowing biocompatibility by shielding the cationic micelles, which can be detached under the tumor acidic microenvironment and facilitates the cellular uptake; (2) polypeptide polylysine-polyphenylalanine (PKF) synthesized *via* ring-opening polymerization for micelle formation and CPT analogue loading; (3) dimeric CPT (DCPT) with redox-sensitive linker for increasing CPT loading and ensuring drug release at tumor sites. Interestingly, the linear-like morphology of PEG-PKF/DCPT micelles was able to enhance their cellular internalization when compared with the spherical blank PKF micelles. Also, the anticancer efficacy of DCPT against lung cancer cells was significantly improved by the micelle formation. In conclusion, this work provides a promising strategy facilitating the safety and effective application of CPT in cancer therapy.

© 2023 Shenyang Pharmaceutical University. Published by Elsevier B.V.
This is an open access article under the CC BY-NC-ND license
(http://creativecommons.org/licenses/by-nc-nd/4.0/)

---

* Corresponding author.
  *E-mail address:* mwchen@um.edu.mo (M.W. Chen).
[1] These authors contributed equally to this work.
  Peer review under responsibility of Shenyang Pharmaceutical University.

# 1. Introduction

Lung cancer is the second most common cancer, which accounts for more than 1.7 million deaths per year [1,2]. Among its various therapeutic regimens, traditional chemotherapy is still the dominant treatment. Camptothecin (CPT), a topoisomerase I (Topo I) inhibitor, is a well-known chemotherapeutic agent and shows anticancer activities in a variety of cancers such as colon, hepatocellular carcinoma, breast and melanoma [3–5]. CPT stabilizes the Topo I-DNA complex, thereby preventing DNA replication and resulting in DNA fragmentation and cell death [6]. However, as previously reported, the clinical application of CPT is greatly hindered by its poor solubility in water [7], rapid lactone-ring hydrolysis [8], and unacceptable side effects such as hemorrhagic cystitis and myelotoxicity [9].

Generally, there are two effective approaches to solve the mentioned issues and realize anticancer effect improvement. One is developing CPT analogues to endow CPT with increased solubility and stability according to the structure-activity relationship [10]. For example, CPT derivatives including topotecan, irinotecan, and belotecan have been prescribed as anticancer drugs. Another approach to improve the anticancer efficacy of CPT is utilizing nanoscale delivery systems, which selectively deliver the cytotoxic CPT into tumor sites. Also, stimuli-responsive nanocarriers can be developed by making use of the pathophysiological changes in cancer tissues such as the pH difference and the alteration of redox status to achieve controlled release [11]. To solve low loading efficiency of CPT, Cai et al. designed a CPT dimer bearing a redox-triggered domain through conjugating two CPT molecules to 2,6-bis(hydroxymethyl)-aniline *via* carbonate linkages. This strategy significantly prevented the self-aggregation and minimized the undesired release of CPT *in vivo* [12]. In addition, Xu et al. designed an exemplified redox-responsive amphiphilic polyprodrug of 10-hydroxycamptothecin (HCPT) *via* polycondensation and "click" chemistry. This system showed merits such as stimuli-responsive bond and rapid chain cleavage [13]. Inspired by these reports, our group previously synthesized a similar DCPT through the reaction between CPT and 2-hydroxyethyl disulfide. Then, this CPT dimer was encapsulated into a targeted polypeptide-based micelle with high loading capacity and redox-triggered release, showing promise for cancer therapy [14]. Though the *in vivo* behaviors of CPT and its analogues have been greatly improved by the single stimulus-responsive nanoscale drug delivery systems, multiple demands of drug delivery or release and combined therapy may not be able to meet. Therefore, multi-stimuli-responsive systems comprising two or more diverse stimulations are desired to improve the delivery of CPT [15].

At present, several multifunctional nano-vehicles including micelles, liposomes, polymers, biopolymers, and dendrimers have been proposed to deliver CPT or its derivatives [8]. Among various carriers, polymeric micelles have gained considerable attention in the last few years due to their inherent characteristics such as controllable physicochemical properties [16]. As one of the typical polymers, polypeptides (or poly(amino acids)), constructed by amino acid residues *via* peptide bonds [17], play prominent roles in drug delivery because they not only have the inherent merits of typical polymers as mentioned above, but also possess several unique characteristics [17–21] including non-immunogenicity, excellent biocompatibility and biodegradability, multiple functional groups, distinctive self-assembly behaviors and bioactivities as well as adjustable dosage form. To date, several polypeptides have been designed as vehicles such as micelles or injectable hydrogel to deliver therapeutic molecules for cancer treatment. The frequently used examples include poly(L-lysine), poly(L-leucine), poly(L-alanine), and poly(L-phenylalanine) (PPhe).

Herein, we developed a linear-like polypeptide-based micelle with pH-sensitive detachable PEG to deliver dimeric CPT (DCPT) for the treatment of non-small cell lung cancer (NSCLC). First, PKF polypeptide polymer was synthesized through ring-opening polymerization (ROP) of Lys-NCA and Phe-NCA. Meanwhile, DCPT with a disulfide bond was prepared by the reaction of CPT and 2-hydroxyethyl disulfide as previously reported. This dimer shows the advantages including easy synthesis and stimuli-response like other small molecule prodrugs [22,23]. After the self-assembly of polypeptide and DCPT encapsulation, OHC-PEG-CHO was modified *via* Schiff base reaction to prolong blood circulation, yielding the PEG-PKF/DCPT micelles. Of note, the disulfide linkage of DCPT was prone to be cleaved rapidly under reductive environment, and the Schiff base bond was labile in acidic tumor microenvironment (pH 6.5), showing a pH-responsive PEG detachment, thereby achieving the controlled release of drugs. *In vivo* experimental results indicated that these PEG-PKF/DCPT micelles would be a promising candidate for effective and safe anticancer therapy.

# 2. Materials and methods

## 2.1. Materials

N-$\varepsilon$-carbobenzoxy-L-lysine ($\varepsilon$-Lys(Z)) and L-phenylalanine (Phe) were purchased from GL Biochem Ltd. (Shanghai, China), and lysine-N-carboxylic acid anhydride (Lys(Z)-NCA) and phenylalanine-N-carboxylic acid anhydride (Phe-NCA) were formed according to a previously reported method [24]. CPT was bought from Dalian Meilun Biology Technology Co., Ltd. (Liaoning, China). Hydrogen bromide solution 33 wt% in acetic acid was purchased from J&K Scientific Ltd (Beijing, China). Paraformaldehyde (PFA) and rhodamine B isothiocyanate (Rho) were obtained from Sigma-Aldrich (St. Louis, MO, USA). Poly(ethylene glycol) (MW 6000) was purchased from JenKem Technology Company (Beijing, China), and $\alpha,\omega$-diformyl poly(ethylene glycol) (OHC-PEG-CHO) was prepared by a previously reported one-pot method [25]. Dimethyl sulfoxide (DMSO) and dithiothreitol (DTT) were purchased from Aladdin (Shanghai, China). N, N-dimethylformamide (DMF) was obtained from Damao (Tianjing, China). Pyrene was obtained from Baoman Bio (Shanghai, China). 3-(4,5-Dimethylthiazol-2-yl)-2,5-diphenyltetrazolium bromide (MTT) was obtained from Amresco (Solon, Ohio, USA). An Annexin V-FITC early apoptosis detection kit,

DAPI, and a JC-1 MMP assay kit were provided by Beyotime Biotechnology (Nantong, China).

## 2.2. Synthesis of polylysine–polyphenylalanine (PKF)

The PKF polypeptide polymer was synthesized by means of ROP, which involves the following steps: Firstly, 0.11 mmol hexylamine as the initiator was added into the solution of Lys(Z)-NCA (1.0 g, 3.27 mmol) in anhydrous DMF (15 ml) at 30 °C for 72 h under a nitrogen flow with stirring to stimulate the reactions of Lys(Z)-NCA to yield the PLys(Z), which was subsequent precipitated by adding excess ether. Secondly, the anhydrous DMF solution of PLys(Z) and Phe-NCA were mixed and reacted at room temperature for 48 h to synthesize PLys(Z)-PPhe, followed by 48 h dialysis (with a molecular weight cut-off of 3500 Da) and lyophilization. Thirdly, the carbobenzoxy groups of PLys(Z)-PPhe were deprotected in trifluoroacetic acid and HBr solution at room temperature, and then precipitated in pre-cooled ether. Finally, the product (PKF) was purified by dialysis after dissolving in DMF. And the dried PKF polypeptide polymer was characterized by $^1$H nuclear magnetic resonance spectroscopy (Bruker, USA).

## 2.3. Preparation and characterization of PKF/DCPT and PEG-PKF/DCPT micelles

DCPT was synthesized as previously reported without modification [14,26]. Briefly, 696 mg CPT was suspended in anhydrous DCM (30 ml). Then, 237 mg triphosgene and 244 mg DMAP were added to the suspension. The mixture was stirred at room temperature for 4 h until the solution became clear, which was further reacted with 123 mg 2-hydroxyethyl disulfide in THF/DCM (1/3, v/v, 2 ml) and stirred at room temperature for another 24 h. Solvent was then removed, and the crude product was purified by silica gel column chromatography. Mixture of 100 µl PKF (5 mg/ml in DMSO) and 100 µl DCPT (5 mg/ml in DMSO) was slowly added into 2 ml water with constantly stirring. Then, the solution was transferred into a dialysis bag (MWCO: 3500 Da) to fabricate the PKF/DCPT micelles by dialysis method. PEG-PKF/DCPT micelles were obtained by mixing OHC-PEG-CHO (equivalent to 4–6 fold of the mass of PKF) with the PKF/DCPT micelles for 30 min at room temperature with gentle stirring. Then, the particle size and zeta potential of micelles were measured by a Nano-ZS Zetasizer instrument (Malvern, UK), and the morphology of micelles was observed by TEM (Tecnai G2 F20 S-TWIN, Tecnai, USA). Furthermore, the CPT concertation in micelles were determined by HPLC (Waters e2695, USA) at a maximum absorbance of 380 nm to calculate the loading capacity (DL) and encapsulation efficiency (EE) following a previously reported method [14]. In addition, PKF blank micelles and PEG-PKF blank micelles were constructed via the same approach without the addition of DCPT.

## 2.4. pH-sensitive PEG detachment

The zeta potential of micelles in PBS with different pH was compared to verify the pH-sensitive PEG detachment. In short, 1 ml of the prepared micelles were cultured with 1 ml PBS (pH

7.4 or 6.5, 20 mM) for 10 min. The changes of zeta potential were recorded.

## 2.5. Stability

The stability of PKF/DCPT and PEG-PKF/DCPT micelles was evaluated by comparing the alterations of the particle sizes and zeta potentials incubated with pH 7.4 PBS in a 37 °C orbital shaker incubator at various predetermined time points (PBS: 0, 0.5, 1, 4, 8, 24 h), the mean particle sizes and zeta potentials of these treated micelles were recorded.

## 2.6. Critical micelle concentration (CMC)

To investigate the CMC of PEG-PKF blank micelles, a commonly used fluorescence probe, pyrene ($6.0 \times 10^{-7}$ mol/l), was added into PEG-PKF blank micelles with various concentrations ($2 \times 10^{-6}$ mg/ml to 1 mg/ml) and incubated at room temperature overnight. The pyrene fluorescence of all samples at wavelengths of 373 ($I_{373}$) and 384 nm ($I_{384}$) were recorded by using a fluorescence spectrometer (Thermo, USA). Then, the intensity ratios ($I_{373}/I_{384}$) were calculated and plotted against the logarithm of the concentrations. The CMC was analyzed by cross-point linear regressions.

## 2.7. Gel permeation chromatography (GPC)

GPC was performed to determine the molecular weight and molecular weight distribution of PKF and PEG-PKF micelles by using a Waters Ultrahydrogel 250 mm × 300 mm column with 0.1 M NaNO$_3$ as mobile phase (0.8 ml/min) and PEG1000-218000 was used as a standard for column calibration. Samples were analyzed with a refractive index detector (Waters 2414, USA).

## 2.8. Fourier transform infrared spectroscopy (FTIR)

For IR analysis, the pellets were prepared by grinding 1 to 2 mg sample and 200 mg potassium bromide. IR spectra were obtained in the range of 400 to 4000 cm$^{-1}$.

## 2.9. In vitro drug release

To investigate the release behavior of CPT from PEG-PKF/DCPT micelles, 1 ml micelles was added to a dialysis bag (MWCO = 3500 Da) against 20 ml of different media including PBS (pH 7.4 or pH 6.5) with or without DTT (10 mM). All these groups were placed in a shaker incubator. The sample was collected at predetermined time points and then replaced with the same volume of corresponding fresh medium. The CPT content was measured by HPLC, and the kinetic release profiles of CPT were then calculated.

## 2.10. Cell culture

Human lung adenocarcinoma epithelial cell line A549 and human large cell lung cancer cell line NCI-H460 were supplied by American Type Culture Collection (ATCC, Rockville, MD, USA) and cultured in high-glucose Dulbecco's modified Eagle's

medium (DMEM, Grand Island, USA) containing 10% (v/v) heat-inactivated fetal bovine serum (FBS), 100 units/ml penicillin, and 100 µg/ml streptomycin in a 5% $CO_2$ incubator at 37 °C. The cell lines used for experiments were within 20 passages.

### 2.11. Endocytosis efficiency

To compare the endocytosis efficiency of spherical micelles and linear micelles in A549 and NCI-H460 NSCLC cells, Rho was employed to core-label the sphere-shaped PKF and PEG-PKF blank micelles, as well as the PKF/DCPT and PEG-PKF/DCPT micelles. First, A549 and NCI-H460 cells were seeded in 6-well plates at a density of $2.0 \times 10^5$ cells per well and incubated for 24 h. Later, DMEM (pH 7.4 or 6.5) containing Rho-labeled micelles at an equivalent Rho concentration of 2 µg/ml were added to the cells. After 6 h incubation at 37 °C, the cells were collected and re-suspended in 400 µl PBS (pH 7.4). The intracellular fluorescence intensity was quantitated by using a flow cytometer (BD FACS Canto™, USA). To trace the cell internalization of micelles in A549 and NCI-H460 cells, $2.0 \times 10^5$ cells were planted in each confocal petri dish and incubated overnight. Then, the cells were incubated with Rho-labeled micelles at an equivalent Rho concentration of 5 µg/ml in DMEM at different pH values (pH 7.4 or 6.5) for 6 h at 37 °C. Afterward, the cells were washed and fixed with 4% PFA for 15 min and subsequently stained with DAPI (5 µg/ml) for 10 min. Fluorescence images were captured using a Leica TCS SP8 CLSM system (Leica TCS SP8, Germany).

### 2.12. In vitro cytotoxicity

A549 and NCI-H460 cells were seeded in 96-well plates at a density of $8 \times 10^3$ cells per well and then cultured overnight. Then, they were treated with medium (pH 7.4 or 6.5) containing different concentrations of CPT formulations. After 24 h incubation, MTT was added to each well and continued incubating for another 4 h. Furthermore, 100 µl DMSO was added to dissolve the formed formazan crystals, and the absorbance at 570 nm of each well was detected via a microplate reader (SpectraMax M5, Molecular Devices, USA).

### 2.13. Cell apoptosis

The apoptosis-inducing capacity of micelles was evaluated by using an Annexin V-FITC apoptosis detection kit following the manufacturer's instructions. A549 and NCI-H460 cells were planted in 6-well plates and treated with various CPT formulations (equivalent concentration of 10 µM CPT). After 24 h incubation, cells were trypsinized and resuspended in 195 µl binding buffer containing 5 µl Annexin-FITC and 10 µl PI. Finally, flow cytometry (BD FACS Canto™, USA) was conducted to analyze the apoptotic rate induced by the above groups.

### 2.14. Mitochondrial membrane potential (MMP) measurement

MMP was detected with a JC-1 mitochondrial membrane potential assay kit in accordance with manufacturer's instructions. A549 and NCI-H460 cells were seeded in 6-well plates at a density of $2.0 \times 10^5$ cells per well and then treated with CPT formulations at an equivalent CPT concentration of 10 µM. After treatment, the cells were mixed with 1 ml JC-1 staining solution (5 µg/ml) in the dark and incubated for 20 min at 37 °C. After washing twice with PBS, flow cytometry (BD FACS Canto™, USA) was performed to measure the fluorescent intensity.

### 2.15. Animals

Female BALB/C mice (6–7 weeks) and male BALB/c nude mice (5 weeks) were purchased from Gunagdong Medical Laboratory Animal Center (Guangzhou, China). All the experiments were carried out according to the protocols approved by the Academic Ethics Committee of The Zhuhai Campus of Zunyi Medical University.

### 2.16. Pharmacokinetics

Female BALB/C mice were randomly divided into 4 groups ($n = 3$) after fasting (with water) for 24 h. PKF/DCPT and PEG-PKF/DCPT were administered intravenously at the tail vein and DCPT was injected intraperitoneally at an equivalent DCPT dose of 5 mg per kg body weight. The blood samples were collected via tail vein using heparinized blood collecting tubes at predetermined time points (0.5, 1, 2, 4, 6, 8, 12, 24 h), and were stored at −80 °C until analysis. To determine the concentration of DCPT in the collected samples, 10 µl blood was diluted to 50 µl with PBS. Then, fluorescence intensity of CPT was measured by using a SpectraMax microplate reader using excitation wavelength at 370 nm and emission wavelength at 435 nm. The concentration of DCPT in blood was calculated based on the naked DCPT calibration curve.

### 2.17. In vivo therapeutics efficacy evaluation

Human A549 lung cancer-xenografted mouse model was established by subcutaneously injecting $5 \times 10^6$ cells suspended in 100 µl PBS into the right flank of each nude mouse for in vivo therapeutics efficacy evaluation. When the tumor size reached about 100 mm$^3$, the tumor-bearing mice were divided randomly into 4 groups ($n = 5$). The mice were administered with PBS, PKF/DCPT or PEG-PKF/DCPT intravenously or with DCPT intraperitoneally every 2 d, with a total 7 times injection (DCPT dose: 5 mg/kg). The tumor size and body weight were measured every other day. The length (a) and width (b) of the tumors were measured by a vernier caliper and the volume (V) was calculated using the following formular: $V = 0.5 \, ab^2$.

### 2.18. Histopathological analysis

After finishing the therapy, the mice were scarified and the major organs (heart, lung, spleen, kidneys, liver) and tumor were dissected from the mice for histopathological analysis. The tissues or organs were fixed in 10% (w/v) formaldehyde in PBS solution and then embedded in paraffin follow by slicing. Slices with 3 µm thickness were stained with hematoxylin and
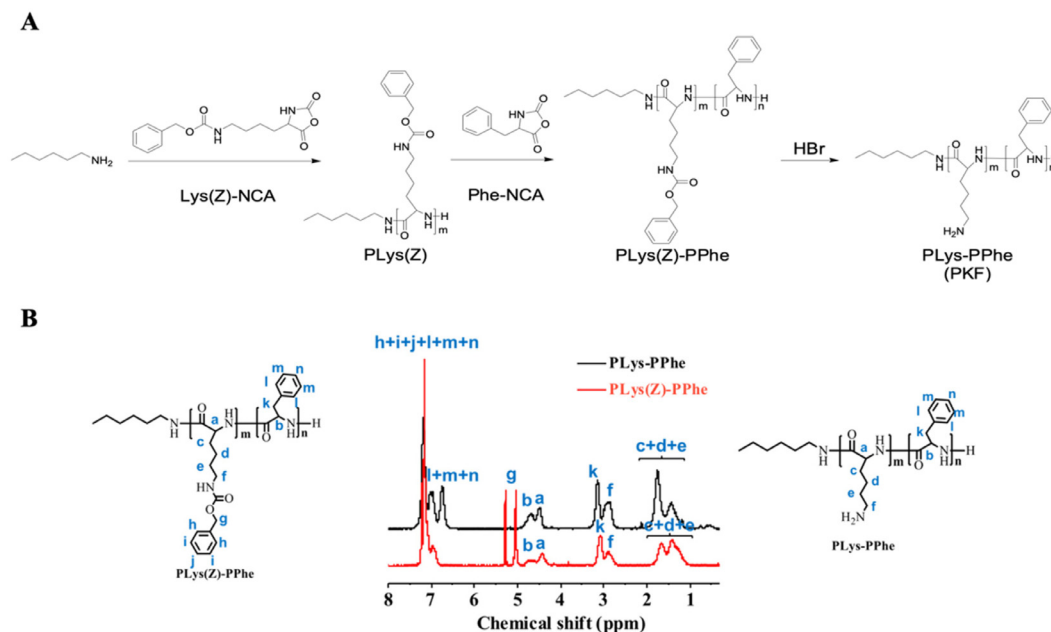
**Fig. 1 – Synthetic pathway (A) and $^1$H-NMR spectra (B) of PLys(Z)-PPhe and PLys-PPhe (PKF).**

eosin (H&E). Finally, the histological changes of tissues were observed using a microscope (BX43, Olympus, Japan).

### 2.19. Statistical analysis

All of the data were presented as the mean ± SD. The statistical difference was analyzed by a two-tailed student's *t*-test. Statistical significance was considered at $P < 0.05$ (denoted by *) and $P < 0.01$ (denoted by **).

## 3. Results and discussion

### 3.1. Synthesis and characterization of PKF and DCPT

PKF polypeptide was synthesized on the basis of a two-step ROP. As illustrated in Fig. 1A, PLys(Z) was first synthesized using hexylamine as an initiator and in turn served as the initiator for the preparation of PLys(Z)-PPhe. Then, PKF was obtained after the removal of protecting groups in PLys(Z)-PPhe. From $^1$H-NMR spectra (Fig. 1B), the peaks (g–j) at about 5.2 ppm and 7.1 ppm were only found in the spectrum of PLys(Z)-PPhe but not PLys-PPhe (PKF) due to the presence of carbobenzoxy groups in PLys(Z)-PPhe. The molecular weight and distribution of PKF were also determined by GPC, showing a unimodal molecular weight distribution (Table. S1). Therefore, it can be confirmed that PKF was successfully synthesized. And the percentage yield was calculated to be 66%. For the synthesis of DCPT, triphosgene was firstly added to CPT for activation, and 2-hydroxyethyl disulfide was added to induce the disulfide linker between CPT molecules. The obtained $^1$H-NMR spectra of DCPT (Fig. S1) was

similar to previous reports. And the percentage yield of DCPT preparation was determined to be 60%.

### 3.2. Preparation and characterization of PKF/DCPT and PEG-PKF/DCPT micelles

Once obtained the PKF polypeptide and DCPT, PKF/DCPT micelles were fabricated by a dialysis method and OHC-PEG-CHO was further modified onto the surface of micelles *via* Schiff base reaction to obtain PEG-PKF/DCPT, in which the PEG groups could be cleaved under weakly acidic environment rapidly. Results showed that the average particle sizes and polydispersity index (PDI) of PKF/DCPT and PEG-PKF/DCPT micelles were 256.2 ± 1.0 nm with PDI 0.19 ± 0.03 and 259.4 ± 1.6 nm with PDI 0.22 ± 0.01 (Fig. 2C&D), respectively, suggesting no obvious morphological changes after coating with PEG. The molecular weight and distribution of PKF/DCPT and PEG-PKF/DCPT were also determined by GPC, further confirming the addition of PEG (Table. S1). Also, PEG-PKF/DCPT micelles possessed high EE and DL, which were determined to be 99% and 51.4%, respectively. Moreover, compared with PKF/DCPT, the zeta potential of PEG-PKF/DCPT micelles significantly decreased from 21.9 ± 1.7 mV to 16.9 ± 0.6 mV, demonstrating the reduced toxicity induced by cationic polymers, but the still positively charged particle surface would contribute to enhanced uptake efficiency [25,27]. Interestingly, the TEM results indicated that PKF blank micelles (PKF-micelle and PEG-PKF-micelle) were spherical, while the DCPT-loaded PKF micelles (PKF/DCPT and PEG-PKF/DCPT) were linear shape (Fig. 2). According to previous reports, the shape of nanoparticles can directly influence their behavior such as the accumulation, penetration, and
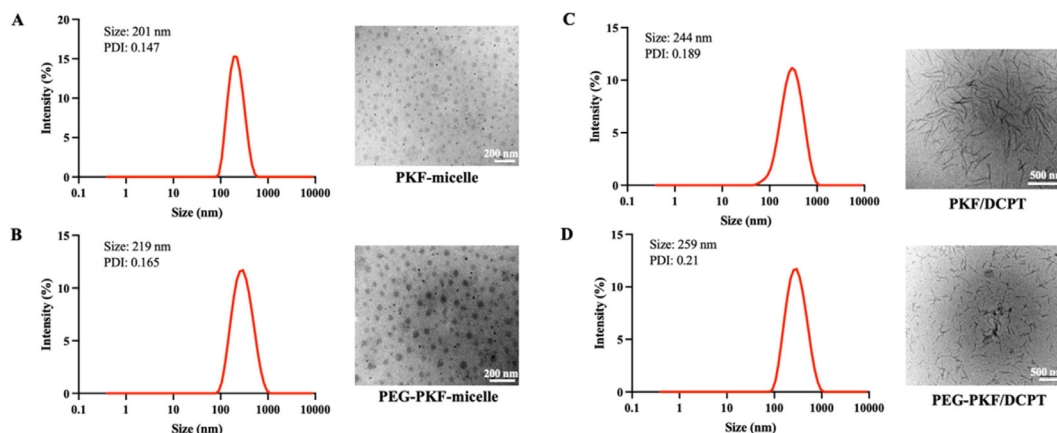
**Fig. 2 – Size distribution and TEM images of PKF micelles (A), PEG-PKF micelles (B), PKF/DCPT micelles (C) and PEG-PKF/DCPT micelles (D).**

cellular uptake. Specifically, linear morphology can reduce the cell capture during blood circulation and possesses better penetration ability than spherical nanoparticles due to the different margination dynamics [28–30]. The observed morphological changes were speculated to result from the hydrogen bond between CPT and PEG-PKF and $\pi$-$\pi$ stacking interaction of CPT itself [31,32]. IR analysis was also performed to investigate the phenomenon (Fig. S2). In addition, TEM images showed that the morphology of DCPT-loaded micelles changed in the presence of GSH, which may be due to the cleavage of S-S bond and disruption of the hydrogen bond and $\pi$-$\pi$ stacking interaction (Fig. S3).

### 3.3. Stability and characteristics of micelles

To validate pH-responsive detachment of PEG, we measured the zeta potentials of PKF/DCPT and PEG-PKF/DCPT micelles at different pH conditions (7.4 or 6.5). As shown in Fig. 3C, the zeta potentials of both micelles were determined to be positive, which should be due to the presence of lysine. In the rational design, lysine was chosen to induce positive charges because of its cationic nature while phenylalanine was introduced to adjust the hydrophobic characteristics of the PKF polypeptide. Meanwhile, the zeta potential of PEG-PKF/DCPT micelles was lower than that of PKF/DCPT micelles at pH 7.4. However, in a weakly acidic environment (pH 6.5), PEG-PKF/DCPT micelles showed similar positive charge to PKF/DCPT. This alternation may be attributed to the cleavage of Schiff base linkage between PEG and PKF polypeptide, which remained stable in physiological condition (pH 7.4) and became labile in acidic tumor microenvironment (pH 6.5). Therefore, such shielding PEG was supposed to be favorable for blood circulation and the subsequent cell uptake for *in vivo* application due to the pH-sensitive cationic charge elevation on the micelle surface [33]. The stabilities of micelles were studied in PBS with pH 7.4. As shown in Fig. 3A and 3B, both the particles size of PKF/DCPT micelles and PEG-PKF/DCPT micelles remained stable in PBS. Consequently, the modification of PEG reduced the positive charge of PKF/DCPT, showing remarkable shielding
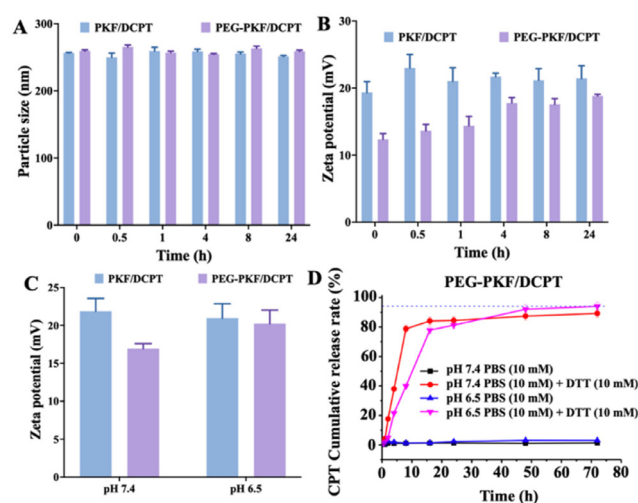


**Fig. 3 – Characterization of PKF/DCPT and PEG-PKF/DCPT micelles. (A) Particle size change of PKF/DCPT and PEG-PKF/DCPT micelles in PBS in 24 h. (B) Zeta potential change of PKF/DCPT and PEG-PKF/DCPT micelles in PBS in 24 h. (C) Zeta potential change of PKF/DCPT and PEG-PKF/DCPT micelles in various pH. (D) *In vitro* release profiles of DCPT in PEG-PKF/DCPT under various conditions.**

ability. Furthermore, as CMC is a crucial parameter to characterize the self-assemble stability of micelles [34], the CMC value of PEG-PKF/DCPT micelles was measured by pyrene fluorescence probe spectrometry and found to be 0.0121 mg/ml (Fig. S4), suggesting their strong ability to maintain the structure in diluted conditions. Together with its pH-responsive characteristics, PEG-PKF/DCPT might be a promising therapeutic in further application. Furthermore, the *in vitro* release profiles of CPT from PEG-PKF/DCPT micelles or PKF-DCPT were investigated in PBS (pH 7.4 or 6.5) with or without DTT. As shown in Figs. 3D and S5, in the absence of DTT, micelles remained stable and exhibited almost no CPT release regardless of the pH difference. However, in PBS with 10 mM DTT, micelles showed rapid release, with cumulative
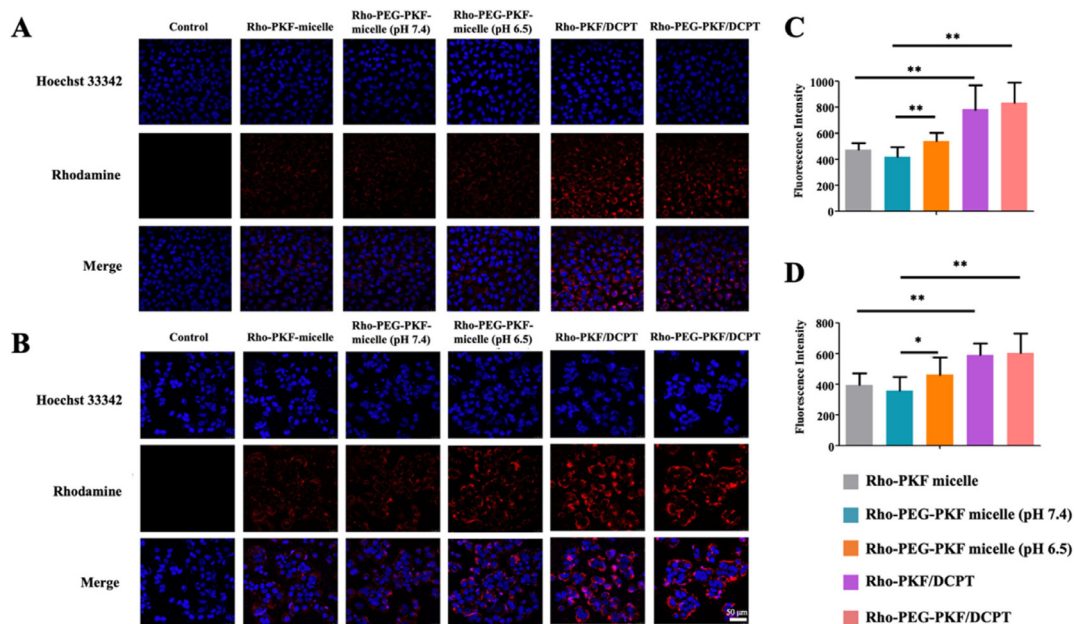
**Fig. 4 – Confocal microscopy images and flow cytometry analysis to study the cellular uptake of micelles in A549 cells (A, C) and NCI-H460 cells (B, D), scale bar is 50 μm.**

release of 89.2% (pH 7.4) and 94.1% (pH 6.5) in PEG-PKF/DCPT groups. This result proved the redox-triggered release of DCPT-loaded micelles.

### 3.6. Cellular uptake

Rod-like micelles are superior in cell internalization than sphere-shaped micelles [35]. To verify this point, spherical PKF blank micelles (PKF-micelle and PEG-PKF-micelle) and linear-like DCPT-loaded micelles (PKF/DCPT and PEG-PKF/DCPT) were labeled with Rho to enable them to be detected by flow cytometry and visualized through CLSM. Compared with the uptake efficiency in the medium of pH 7.4, sphere-shaped PEG-PKF-micelle exhibited slightly enhanced cellular uptake in the medium of pH 6.5 (Fig. 4C and 4D), which was contributed to the pH-sensitive PEG detachment. Importantly, linear-shaped PKF/DCPT and PEG-PKF/DCPT micelles exerted significantly increased endocytosis efficiency than corresponding spherical PKF blank micelles, proving that linear-like micelles have stronger cellular uptake than spherical micelles. Meanwhile, PKF/DCPT and PEG-PKF/DCPT micelles also displayed strong red fluorescence intensity of Rho in CLSM images (Fig. 4A and 4B), which was consistent with the results of flow cytometry analysis.

### 3.7. In vitro cytotoxicity

MTT assays were conducted to investigate the toxic effects of various CPT formulations against A549 and NCI-H460 cells. Firstly, negligible damages were observed in either PKF or PEG-PKF-treated groups, suggesting the excellent biocompatibility of PKF (Fig. 5A). As shown in Fig. 5B, PKF/DCPT and PEG-PKF/DCPT micelles induced much lower cell viabilities than free CPT, indicating that this kind DCPT-loaded micelle

helped to improve the anticancer effects of CPT. The similar cytotoxicity between these two DCPT-loaded micelles may be due to the similar uptake efficacy. Given that DCPT eventually converted to CPT to exert inhibitory effects, the cell viabilities of CPT-treated and DCPT-treated groups were also similar in both cells. The IC50 of the DCPT formulations were below 2 μM, which showed similar therapeutic efficacy as compared to previous results in lung cancer cell lines treatment [36].

### 3.8. Cell apoptosis

Apoptosis analysis was performed to further assess whether the enhanced cellular internalization of DCPT-loaded micelles would result in improved antitumor activity. As expected, PKF/DCPT and PEG-PKF/DCPT micelles induced 45.73% and 42.41% apoptotic cell death in A549 cells (Fig. 6A), respectively, which were 2.03- and 1.88-fold greater than that of CPT and 1.55- and 1.44-fold greater than that of DCPT, respectively. Similarly, the number of apoptotic NCI-H460 cells treated with PEG-PKF/DCPT micelles was also obviously higher than that of the CPT group (Fig. 6B). The elevated apoptosis rates may result from the enhanced cellular internalization and subsequent rapid drug release triggered by GSH, suggesting the high efficiency of the linear-like DCPT loaded micelles.

### 3.9. MMP measurement

Given that mitochondria play a key role in tumor progression [37], mitochondrial function in cell apoptosis induced by CPT, DCPT, and DCPT-loaded micelles was evaluated utilizing MMP-sensitive JC-1 probe. In NCI-H460 cells (Fig. 7B), free CPT and free DCPT decreased the JC-1 red/green fluorescence intensity to 65.79% and 57.29% of the control ratio, whereas PKF/DCPT and PEG-PKF/DCPT micelles induced a loss of MMP by 47.36%
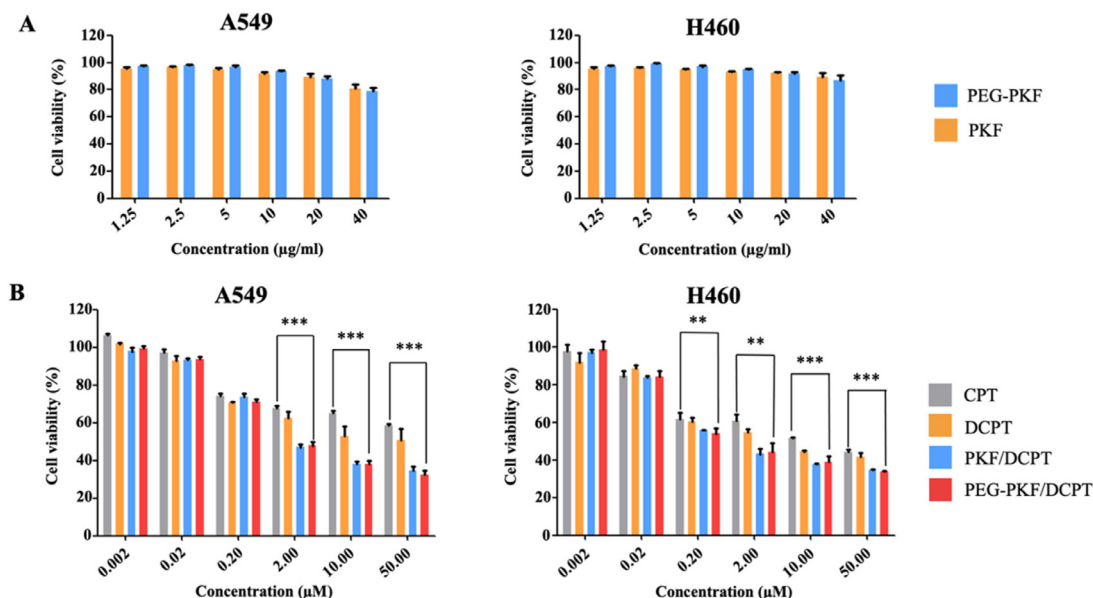
**Fig. 5 – *In vitro* cytotoxicity of PKF and PEG-PKF (A) and various CPT formulations (B) in A549 cells and NCI-H460 cells.**
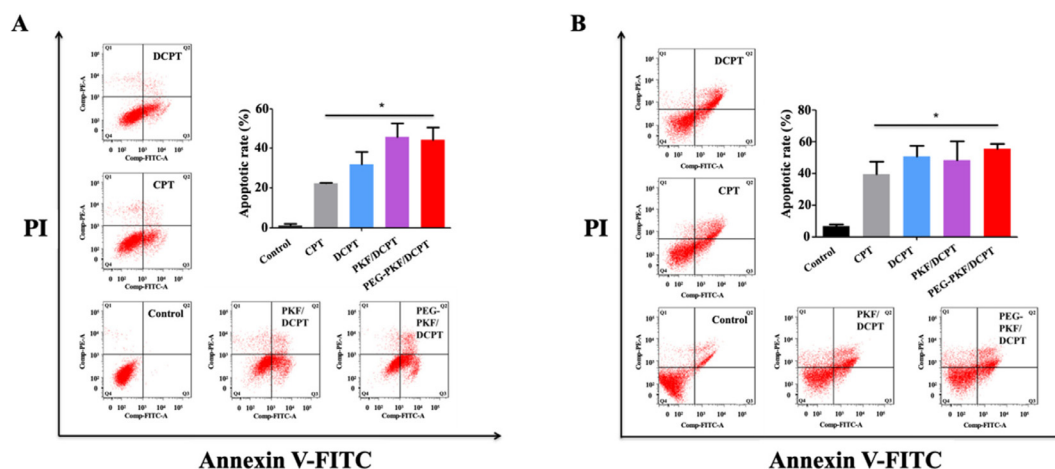


**Fig. 6 – Quantitative measurement of apoptosis rates of A549 (A) and NCI-H460 (B) cells treated with free CPT, free DCPT, PKF/DCPT, and PEG-PKF/DCPT micelles for 24 h. The apoptosis rate was calculated as the sum of the early apoptosis rate and late apoptosis rate. Q1: necrotic cells (Annexin V-FITC− PI+); Q2: late apoptotic cells (Annexin V-FITC+ PI+); Q3: live cells (Annexin V-FITC− PI−); Q4: early apoptotic cells (Annexin V-FITC+ PI−).**

and 47.50%, respectively. Similar results were observed in A549 cells (Fig. 7A). These results indicated that CPT, especially PEG-PKF/DCPT micelles, markedly decreased the MMP and induced early cell apoptosis.

### 3.10. Pharmacokinetics, in vivo tumor treatment, and histological analyses

The pharmacokinetic profiles of DCPT, PKF/DCPT and PEG-PKF/DCPT were compared and studied (Fig. 8A). The concentration of DCPT in blood decreased significantly, which was consistent with previous report that naked CPT was

cleared quickly after administration. The concentration of DCPT in blood was significantly improved in PKF/DCPT or PEG-PKF/DCPT micelles. And the DCPT concentration in PEG-PKF/DCPT was slightly higher than that of PKF/DCPT, which may be due to the presence of CHO-PEG-CHO. The improved blood concentration of PKF/DCPT or PEG-PKF/DCPT may be attributed to the positive charge, which combined with negatively-charged serum proteins after injecting into the blood.

*In vivo* anti-cancer evaluation was carried out to further investigate the potential use of PKF-DCPT and PEG-PKF/DCPT. As shown in Fig. 8C, the tumor growth was significantly
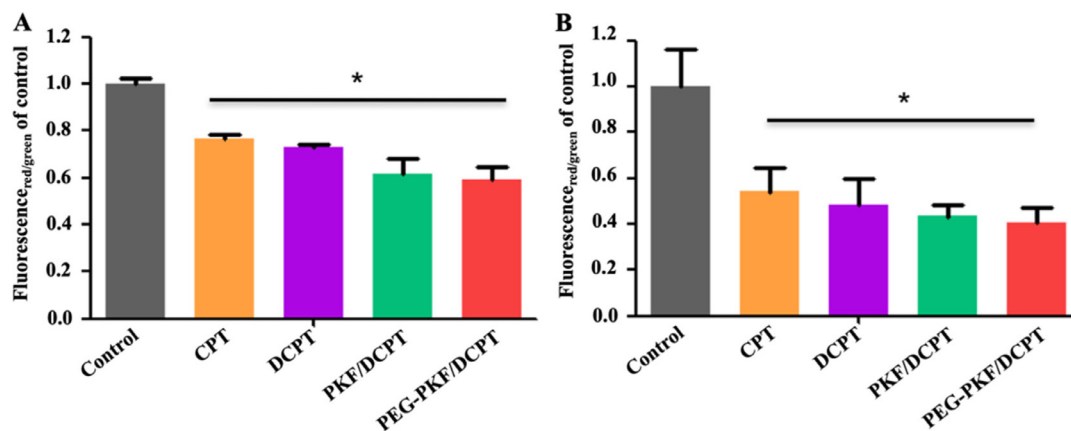
**Fig. 7 – Flow cytometry analysis of fluorescence intensity of JC-1 probe in A549 (A) and NCI-H460 (B) cells for MMP measurement.**
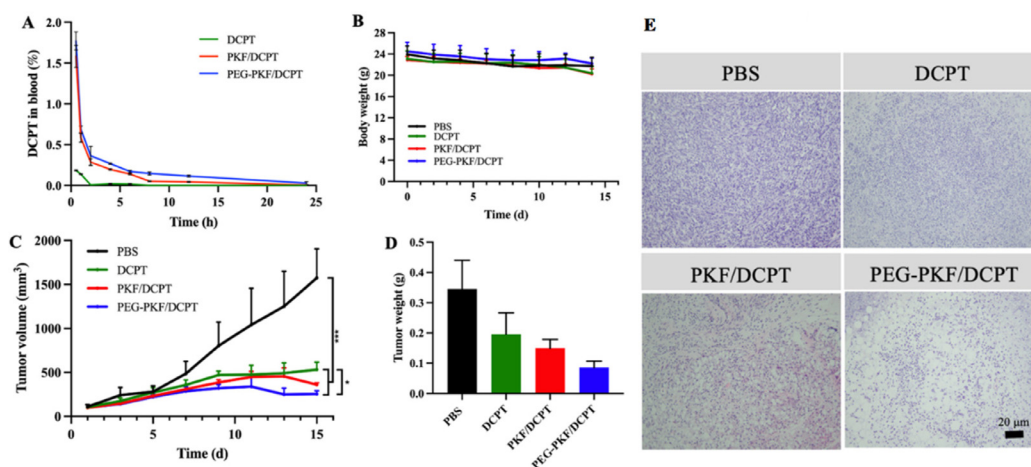


**Fig. 8 – *In vivo* anti-tumor therapy. (A) Concentration of DCPT in blood at different predetermined time point after intravenous injection of PKF/DCPT and PEG-PKF/DCPT) or intraperitoneal injection of DCPT in mice (5 mg/kg of DCPT concentration, *n* = 3); (B) body weight of mice during treatment (*n* = 5); (C) tumor volume changes during treatment (*n* = 5); (D) Tumors weight of each group after treatment (*n* = 5); (E) H&E staining images of tumor collected from DCPT treatment group and PBS group, scale bar is 20 μm.**

suppressed in all treatment groups as compared to the control group. PEG-PKF/DCPT showed the strongest tumor inhibition with an average tumor size around 300 mm$^3$, which was in accordance with the cell apoptosis results (Fig. 8C–8E).

The body weight of mice treated with various DCPT showed a decrease trend similar to that of PBS treatment groups (Fig. 8B). For PBS control group, the body weight loss should be affected by the progression of tumor growth. For CPT formulations group, the body weight loss may be related to the potential anti-obesity ability of CPT [38]. H&E-stained tissue sections from the major organs demonstrated that the DCPT formulations did not damage or show toxicity to the organs (Fig. 9). According to *in vivo* antitumor therapy results, PKF-DCPT and PEG-PKF-DCPT showed high efficiency in tumor suppression, which may attribute to their deeper tumor penetration.

### 3.11.    *Discussion*

In this work, a linear-like polypeptide-based micelle (PEG-PKF/DCPT) with a pH-sensitive detachable PEG shell was fabricated to physically encapsulate redox-responsive DCPT for NSCLC treatment. To form the micelle, PKF polypeptide polymer was constructed chemically through ring-opening polymerization of Lys-NCA and Phe-NCA while DCPT was synthesized by inducing a disulfide linker. This system combines the advantages of easy micelle preparation and stimuli-responsive chemical bonds and structures to achieve the controlled release of drugs, which are important factors in the development of drug delivery systems [39]. The particle size and zeta potential of prepared PEG-PKF/DCPT micelles were measured as 259.4 ± 1.6 nm with PDI 0.22 ± 0.01 and 16.9 ± 0.6 mV, which attained higher tumor accumulation *via*
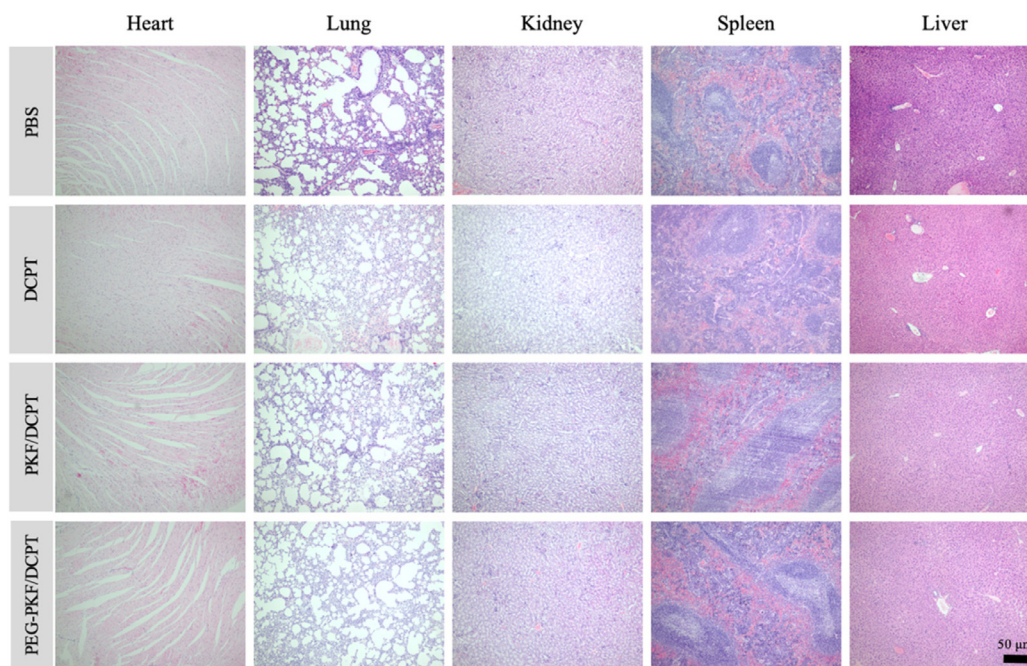
**Fig. 9 – H&E staining of major organs (heart, lung, kidneys, spleen and liver) collected from one mouse after treatment, scale bar is 50 μm.**

EPR effects and enhanced the cell uptake efficiency due to the positive charge. Moreover, OHC-PEG-CHO showed pH-dependent detachment owing to the cleavage of Schiff base linkage between PEG and PKF polypeptide in acidic tumor microenvironment (pH 6.5), thus increasing the positive zeta potential and endocytosis efficiency of micelles. And the linear-shaped PKF/DCPT and PEG-PKF/DCPT micelles also exerted obviously increased endocytosis efficiency than spherical PKF blank micelles. The rapid release of DCPT from micelles was sensitive to the ROS overexpression in tumor sites, which showed significant *in vitro* cytotoxicity against A549 and NCI-H460 cells. In pharmacokinetics study, the concentration of DCPT in blood was significantly improved in PKF/DCPT or PEG-PKF/DCPT micelles, and PEG-PKF/DCPT showed the best *in vivo* antitumor activities. More importantly, the positively-charged units of PKF-DCPT and PEG-PKF-DCPT had little effect on their blood circulation and safety profiles, which is beneficial for efficient and safe anticancer therapies.

## 4. Conclusion

A linear-like polypeptide-based micelle with pH-sensitive detachable PEG (PEG-PKF/DCPT) was successfully developed to deliver DCPT for the treatment of NSCLC. The obtained PEG-PKF/DCPT micelles possessed suitable particle size, positive zeta potential, linear-shaped morphology, and excellent stability. Upon acidic environment, the PEG shell of PEG-PKF/DCPT micelles was detached and led to the increase of zeta potential. Under reductive conditions, CPT rapidly released from the micelles. Importantly, compared with sphere-shaped PKF blank micelles, the linear-like DCPT-loaded micelles exerted significantly improved uptake efficiency in A549 and NCI-H460 cells. Furthermore, *in vitro* and *in vivo* studies confirmed the satisfactory antitumor effects of PEG-PKF/DCPT micelle due to its prolonged blood circulation, enhanced tumor accumulation, and redox-responsive drug release. The results of this study revealed that PEG-PKF/DCPT micelle is a potential strategy for improved clinical CPT outcome in lung cancer therapy.

## Conflicts of Interest

The authors report no conflicts of interest.

## Acknowledgments

## Supplementary materials

Supplementary material associated with this article can be found, in the online version, at doi:10.1016/j.ajps.2022.100773.

## References

[1] Hirsch FR, Scagliotti GV, Mulshine JL, Kwon R, Curran WJ, Wu YL, et al. Lung cancer: current therapies and new targeted treatments. Lancet 2017;389(10066):299–311.

[2] Thai AA, Solomon BJ, Sequist LV, Gainor JF, Heist RS. Lung cancer. Lancet N Am Ed 2021;398(10299):535–54.

[3] Qu Y, Chu B, Wei X, Lei M, Hu D, Zha R, et al. Redox/pH dual-stimuli responsive camptothecin prodrug nanogels for "on-demand" drug delivery. J Control Release 2019;296:93–106.

[4] Zahiri M, Taghdisi SM, Abnous K, Ramezani M, Alibolandi M. Fabrication of versatile targeted lipopolymersomes for improved camptothecin efficacy against colon adenocarcinoma *in vitro* and *in vivo*. Expert Opin Drug Deliv 2021;18(9):1309–22.

[5] Landgraf M, Lahr CA, Kaur I, Shafiee A, Sanchez-Herrero A, Janowicz PW, et al. Targeted camptothecin delivery via silicon nanoparticles reduces breast cancer metastasis. Biomaterials 2020;240:119791.

[6] Acevedo-Morantes CY, Acevedo-Morantes MT, Suleiman-Rosado D, Ramírez-Vick JE. Evaluation of the cytotoxic effect of camptothecin solid lipid nanoparticles on MCF7 cells. Drug Deliv 2013;20(8):338–48.

[7] Basili S, Moro S. Novel camptothecin derivatives as topoisomerase I inhibitors. Expert Opin Ther Pat 2009;19(5):555–74.

[8] Botella P, Rivero-Buceta E. Safe approaches for camptothecin delivery: structural analogues and nanomedicines. J Control Release 2017;247:28–54.

[9] Zunino F, Pratesi G. Camptothecins in clinical development. Expert Opin Investig Drugs 2004;13(3):269–84.

[10] Kim DK, Lee N. Recent advances in topoisomerase I-targeting agents, camptothecin analogues. Mini Rev Med Chem 2002;2(6):611–19.

[11] Fan Z, Jiang C, Wang Y, Wang K, Marsh J, Zhang D, et al. Engineered extracellular vesicles as intelligent nanosystems for next-generation nanomedicine. Nanoscale Horiz 2022;7(7):682–714.

[12] Cai K, He X, Song Z, Yin Q, Zhang Y, Uckun FM, et al. Dimeric drug polymeric nanoparticles with exceptionally high drug loading and quantitative loading efficiency. J Am Chem Soc 2015;137(10):3458–61.

[13] Xu XD, Cheng YJ, Wu J, Cheng H, Cheng SX, Zhuo RX, et al. Smart and hyper-fast responsive polyprodrug nanoplatform for targeted cancer therapy. Biomaterials 2016;76:238–49.

[14] Guo Z, Zhou X, Xu M, Tian H, Chen X, Chen M. Dimeric camptothecin-loaded RGD-modified targeted cationic polypeptide-based micelles with high drug loading capacity and redox-responsive drug release capability. Biomater Sci 2017;5(12):2501–10.

[15] Fu Q, Li Z, Fu F, Chen X, Song J, Yang H. Stimuli-responsive plasmonic assemblies and their biomedical applications. Nano Today 2021;36:101014.

[16] Yokoyama M. Polymeric micelles as drug carriers: their lights and shadows. J Drug Target 2014;22(7):576–83.

[17] He C, Zhuang X, Tang Z, Tian H, Chen X. Stimuli-sensitive synthetic polypeptide-based materials for drug and gene delivery. Adv Healthc Mater 2012;1(1):48–78.

[18] Song Z, Han Z, Lv S, Chen C, Chen L, Yin L, et al. Synthetic polypeptides: from polymer design to supramolecular assembly and biomedical application. Chem Soc Rev 2017;46(21):6570–99.

[19] Cai C, Lin J, Lu Y, Zhang Q, Wang L. Polypeptide self-assemblies: nanostructures and bioapplications. Chem Soc Rev 2016;45(21):5985–6012.

[20] Huang J, Heise A. Stimuli responsive synthetic polypeptides derived from N-carboxyanhydride (NCA) polymerisation. Chem Soc Rev 2013;42(17):7373–90.

[21] Ren X, Wang N, Zhou Y, Song A, Jin G, Li Z, et al. An injectable hydrogel using an immunomodulating gelator for amplified tumor immunotherapy by blocking the arginase pathway. Acta Biomater 2021;124:179–90.

[22] Meng Q, Hu H, Zhou L, Zhang Y, Yu B, Shen Y, et al. Logical design and application of prodrug platforms. Polym Chem 2019;10(3):306–24.

[23] Meng Q, Hu H, Jing X, Sun Y, Zhou L, Zhu Y, et al. A modular ROS-responsive platform co-delivered by 10-hydroxycamptothecin and dexamethasone for cancer treatment. J Control Release 2021;340:102–13.

[24] Semple JE, Sullivan B, Sill KN. Large-scale synthesis of $\alpha$-amino acid-N-carboxyanhydrides. Synth Commun 2017;47(1):53–61.

[25] Guan XW, Guo ZP, Lin L, Chen J, Tian HY, Chen XS. Ultrasensitive pH triggered charge/size dual-rebound gene delivery system. Nano Lett 2016;16(11):6823–31.

[26] Wang H, Xu M, Xiong M, Cheng J. Reduction-responsive dithiomaleimide-based nanomedicine with high drug loading and FRET-indicated drug release. Chem Commun 2015;51(23):4807–10.

[27] Tian H, Guo Z, Lin L, Jiao Z, Chen J, Gao S, et al. pH-responsive zwitterionic copolypeptides as charge conversional shielding system for gene carriers. J Control Release 2014;174:117–25.

[28] Müller K, Fedosov DA, Gompper G. Margination of micro- and nano-particles in blood flow and its effect on drug delivery. Sci Rep 2014;4(1):4871.

[29] Geng Y, Dalhaimer P, Cai S, Tsai R, Tewari M, Minko T, et al. Shape effects of filaments *versus* spherical particles in flow and drug delivery. Nat Nanotechnol 2007;2(4):249–55.

[30] Guo Z, Hu Y, Zhao M, Hao K, He P, Tian H, et al. Prodrug-based versatile nanomedicine with simultaneous physical and physiological tumor penetration for enhanced cancer chemo-immunotherapy. Nano Lett 2021;21(9):3721–30.

[31] Kasai H, Murakami T, Ikuta Y, Koseki Y, Baba K, Oikawa H, et al. Creation of pure nanodrugs and their anticancer properties. Angew Chem Int Ed 2012;51(41):10315–18.

[32] He DX, Zhang W, Deng HZ, Huo SD, Wang YF, Gong NQ, et al. Self-assembling nanowires of an amphiphilic camptothecin prodrug derived from homologous derivative conjugation. Chem Commun 2016;52(98):14145–8.

[33] Sun CY, Shen S, Xu CF, Li HJ, Liu Y, Cao ZT, et al. Tumor acidity-sensitive polymeric vector for active targeted siRNA delivery. J Am Chem Soc 2015;137(48):15217–24.

[34] Liu J, Pang Y, Huang W, Zhu X, Zhou Y, Yan D. Self-assembly of phospholipid-analogous hyperbranched polymers nanomicelles for drug delivery. Biomaterials 2010;31(6):1334–41.

[35] Li D, Tang Z, Gao Y, Sun H, Zhou S. A bio-inspired rod-shaped nanoplatform for strongly infecting tumor cells and enhancing the delivery efficiency of anticancer drugs. Adv Funct Mater 2015;26(1):66–79.

[36] Guo Z, Lin L, Hao K, Wang D, Liu F, Sun P, et al. Helix Self-assembly behavior of amino acid-modified camptothecin prodrugs and its antitumor effect. ACS Appl Mater Interfaces 2020;12(6):7466–76.

[37] Zong WX, Rabinowitz JD, White E. Mitochondria and cancer. Mol Cell 2016;61(5):667–76.

[38] Lu JF, Zhu MQ, Xie BC, Shi XC, Liu H, Zhang RX, et al. Camptothecin effectively treats obesity in mice through GDF15 induction. PLoS Biol 2022;20(2):e3001517.

[39] Meng QY, Cong HL, Hu H, Xu FJ. Rational design and latest advances of codelivery systems for cancer therapy. Mater Today Bio 2020;7:100056.